

The TOTEM experiment

V. Avati^{2,6}, V. Bergholm⁶, V. Boccone⁴, M. Bozzo⁴, M. Buenerd⁵, A. Buzzo⁴, R. Cereseto⁴, S. Cuneo⁴, C. Da Viá¹, M. Deile², K. Eggert², F. Ferro⁴, J.P. Guillaud⁹, J. Hasi¹, F. Haug², R. Herzog³, P. Jarron², J. Kalliopuska⁶, A. Kiiskinen⁷, K. Kurvinen⁷, A. Kok¹, W. Kundrat⁸, R. Lauhakangas⁷, M. Lokajicek⁸, D. Macina², M. Macrí⁴, T. Mäki⁷, S. Minutoli⁴, A. Morelli⁴, P. Musico⁴, M. Negri⁴, E. Noschis^{2,7}, F. Oljemark⁶, R. Orava^{6,7}, M. Oriunno², K. Österberg⁶, V.G. Palmieri⁶, K. Protasov⁵, R. Puppò⁴, D. Rebreyend⁵, R. Rudischer³, G. Ruggiero², H. Saarikko^{6,7}, A. Santroni⁴, G. Sanguinetti¹⁰, G. Sette⁴, W. Snoeys², S. Tapprogge⁷, A. Toppinen⁶, A. Verdier², S. Watts¹, and E. Wobst³

¹ Electronic and Computer Engineering Department, Brunel University, Uxbridge (United Kingdom)

² CERN, Geneva, (Switzerland)

³ ILK, Institut für Luft und Kältetechnik, Dresden, (Germany)

⁴ INFN Sez. di Genova and Università di Genova, Genoa (Italy) e-mail: m.bozzo@ge.infn.it

⁵ Institut des Sciences Nucléaires, IN2P3, Grenoble, (France)

⁶ High Energy Physics Division, Department of Physical Sciences, University of Helsinki, Helsinki (Finland)

⁷ Helsinki Institute of Physics, Helsinki (Finland)

⁸ Institute of Physics, Academy of Sciences of the Czech Republic, Praha (Czech Republic)

⁹ LAPP Annecy, (France)

¹⁰ INFN Sez. di Pisa, Pisa (Italy)

Received: 31 July 2003 / Accepted: 10 November 2003 /

Published Online: 13 July 2004 – © Springer-Verlag / Società Italiana di Fisica 2004

Abstract. TOTEM will measure the total pp cross-section at LHC by using a luminosity independent method based on simultaneous evaluation of the total elastic and inelastic rates. For an extended coverage of the inelastic and diffractive events, two forward tracking telescope are employed. The elastically or diffractively scattered protons are measured by a set of special detectors, which can be moved close to the circulating protons beams. The paper describes the physics reach of the experiment and the detectors which are being considered.

PACS. 2 5.70.Ef – 21.60.Gx – 27.30.+t

1 Introduction

The TOTEM experiment was proposed to measure [1,2]:

- the total cross-section with an absolute error of 1 mbarn by using the luminosity independent method, which requires simultaneous measurements of elastic pp scattering down to the four-momentum transfer squared $-t \sim 10^{-3} \text{ GeV}^2$ and of the inelastic pp interaction rate with an extended acceptance in the forward region. Present extrapolations of the world data to the LHC energy together with the existing cosmic ray data have a typical uncertainty of $\pm 15\%$.
- the elastic pp scattering up to $-t \sim 10 \text{ GeV}^2$
- the diffractive dissociation, including single, double and central diffraction.

Extrapolations of the total cross-section measurements, based on the dispersion relation techniques [3], an estimate of the ρ -parameter [4] and an assumption of $\sigma_{tot} \propto (\log s)^2$, result in about 10% larger σ_{tot} at the

LHC-energies compared to the one obtained by assuming $\sigma_{tot} \propto (\log s)$.

In measuring the total cross-section, one should be especially concerned about the systematics related to the acceptance in measuring the inelastic rate (different detector configurations, Monte Carlo model dependence). The TOTEM experiment is designed to measure σ_{tot} with an accuracy of the order of 1%, which is sufficient to discriminate between the current model predictions for the LHC energy ranging between 100 and 130 mb.

Given the large cross-sections involved, the experiment does not require intense beams, but a special high-beta optics is needed for the measurement of low t elastic scattering. The experiment will be ready to take data at the beginning of the LHC operation and will also provide an absolute luminosity determination.

The TOTEM experiment uses precision detectors inserted in Roman Pots and/or microstation installed in the machine tunnel to measure the elastically and diffractively scattered protons close to the beam direction. Two sepa-

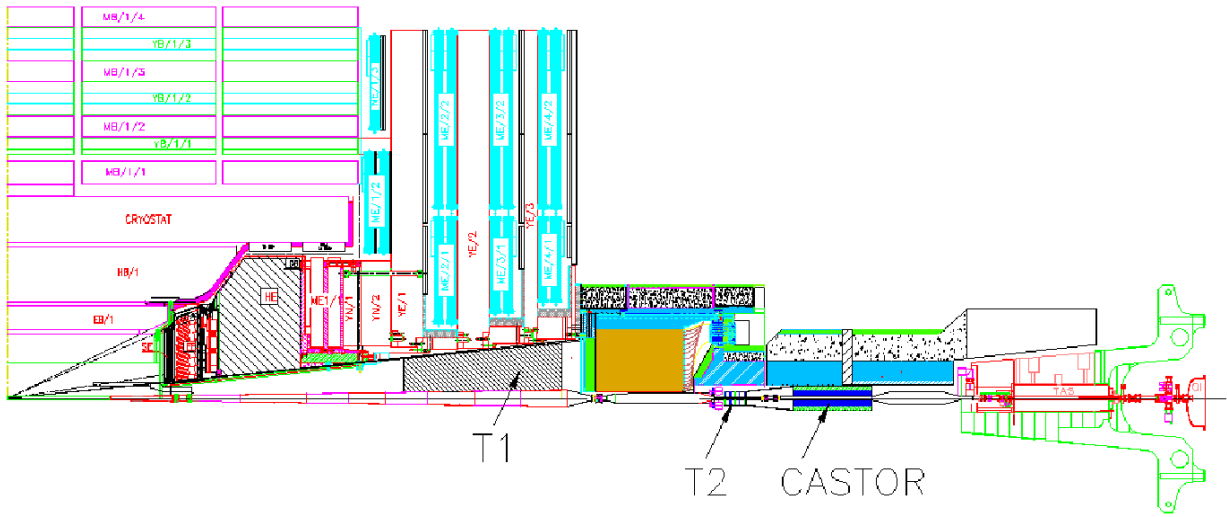


Fig. 1. The TOTEM detectors T1 and T2 installed in the CMS forward region

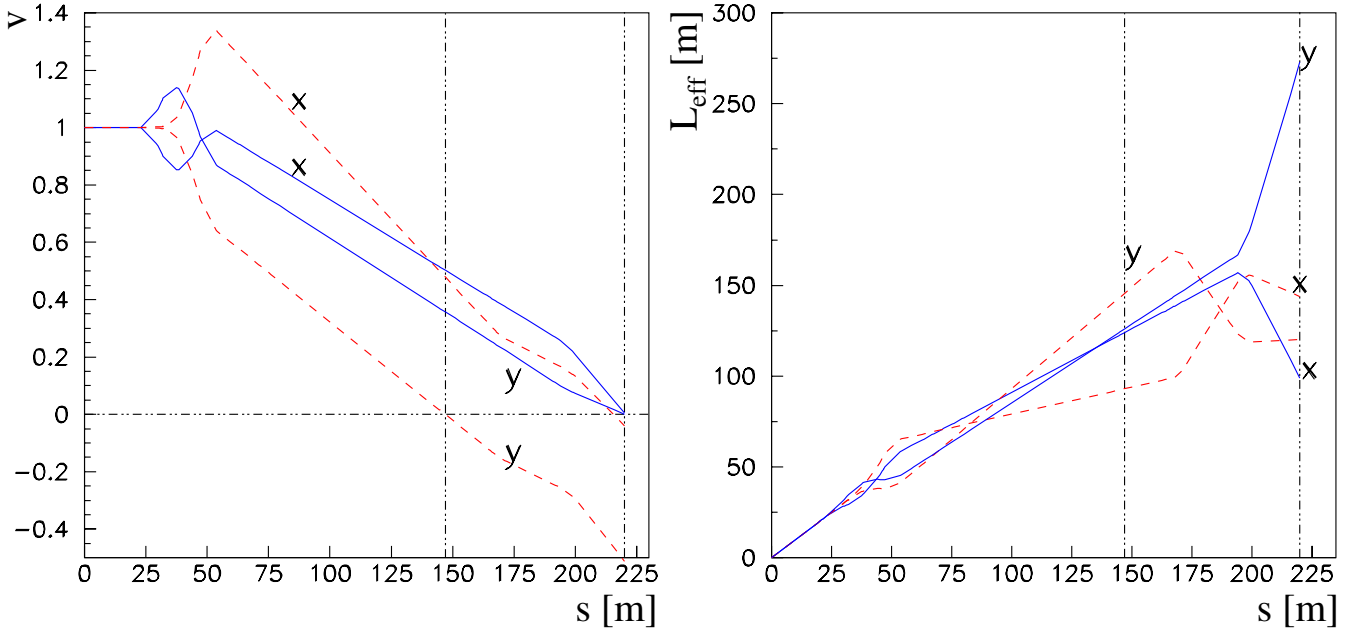


Fig. 2. Magnification v and effective length L_{eff} as a function of the distance from the IP (solid lines $\beta^* = 1540$ m, dashed lines $\beta^* = 1100$ m)

rate forward telescopes will be installed on both sides of the CMS detector with a rapidity coverage of $3 < |\eta| < 6.8$ (Fig. 1). With these additional detectors, a fully inclusive trigger, also for single diffraction, can be provided with an expected loss on the inelastic rate of less than 2%.

The elastic and inelastic interaction rates are related to the integrated luminosity of the machine by the equation:

$$\mathcal{L} \sigma_{tot} = N_{el} + N_{inel} \quad (1)$$

The optical theorem relates the total cross-section to the imaginary part of the forward scattering amplitude lead-

ing to the following equation:

$$\mathcal{L} \sigma_{tot}^2 = \frac{16\pi}{1 + \rho^2} \left(\frac{dN}{dt} \right)_{t=0} \quad (2)$$

Combining the above two equations allows to write the total cross-section as a function of measurable quantities:

$$\sigma_{tot} = \frac{16\pi}{(1 + \rho^2)} \frac{(dN/dt)_{t=0}}{(N_{el} + N_{inel})} \quad (3)$$

Solving (1) and (2) for \mathcal{L} shows that TOTEM will also be able to provide an absolute calibration of the machine luminosity. The ρ parameter with its small value at high

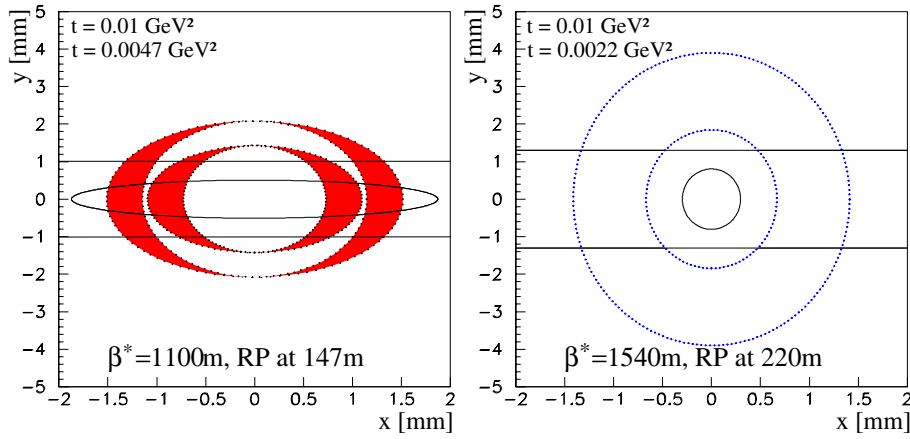


Fig. 4. Contour plots for two t -values for $\beta^* = 1100$ m (left) and $\beta^* = 1540$ m. The 10σ beam envelope and the edge of a detector placed at $10\sigma + 0.5$ mm are also shown

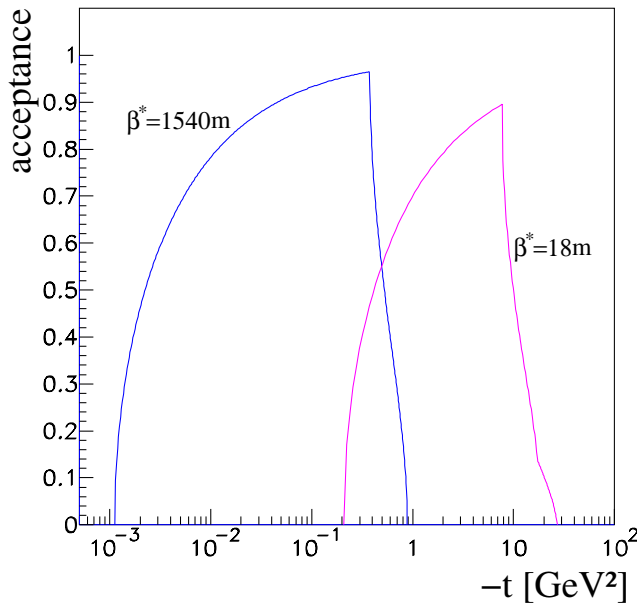


Fig. 5. The acceptance as a function of t for high β^* and for the injection optics

nates on their values at the IP is seen contrary to the original $\beta^* = 1100$ m scheme. The 10σ beam envelope and the vertical location of the edge of a silicon detector 0.5 mm from the beam envelope are also shown.

For $-t > 10^{-3} \text{ GeV}^2$, the proton detection efficiency increases rapidly up to the maximum value of $t \sim 0.5 \text{ GeV}^2$ after which the protons escape the beam pipe (Fig. 5). By using the injection optics of the machine, i.e. $\beta^* = 18$ m, TOTEM will be able to reach $-t$ -values up to 10 GeV^2 . With the nominal number of bunches the luminosity would be $10^{32} \text{ cm}^{-2} \text{ s}^{-1}$ which would allow the high $-t$ measurements to be made within a few short running periods. The acceptance regions of the high- β ($\beta^* = 1540$ m) and injection- β ($\beta^* = 18$ m) overlap at $-t \sim 0.5 \text{ GeV}^2$.

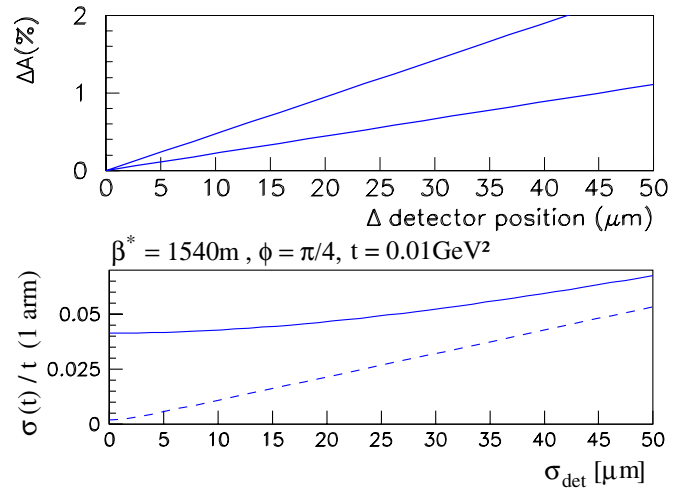


Fig. 6. (top) Acceptance uncertainty versus detector offset for $t = 0.004 \text{ GeV}^2$ (upper curve) and $t = 0.01 \text{ GeV}^2$. (bottom) Relative t -resolution (1 arm only) versus detector resolution (solid), the dotted line shows the ideal case of zero beam divergence (lower curve)

The precision of extrapolation to the optical point ($t = 0$) critically depends on the knowledge of the detection efficiency vs. acceptance of the elastically scattered protons. Fig. 6 (top) shows the effect on the acceptance due to the uncertainty in the detector position: special care has to be taken to control systematic effects on the detector position to about $10 \mu\text{m}$. For a total cross-section measurement with 1% precision the acceptance uncertainty for the elastic scattering should be known to 0.5%. Fig. 6 (bottom) shows the relative t -resolution at $-t = 10^{-2} \text{ GeV}^2$; the beam divergence at the IP contributes a 4% error. The detector resolution error (dotted line) has to be added in quadrature. A detector resolution of the order of $30 \mu\text{m}$ is considered to be adequate.

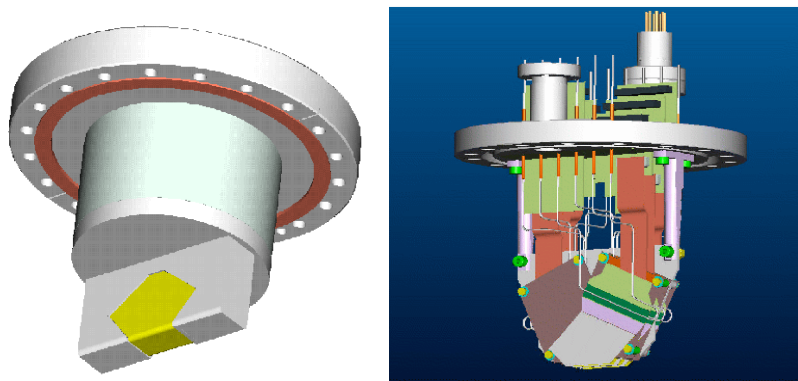


Fig. 7. A schematic view of the TOTEM Roman Pot detector system. The thin window separating the primary beam vacuum and the detector enclosure is seen at the *bottom* of the insertion. The detector arrangement with the front-end electronics and services is shown on the *right*

Table 1. Physics event rates and main backgrounds

	Event Rate (all 4 RP)
Elastic scattering	300 Hz
Single diffraction	200 Hz
Double Pomeron exchange	10 Hz
Beam halo	20 Hz
Beam-gas scattering	< 1 Hz
Photons	\ll 1 Hz

2.1 Level 1 leading proton trigger

The beam-pipe insertions for detecting leading protons (Roman Pots or microstations) will house precision tracking detectors (discussed in Sect. 2.3) and independent level-1 trigger detectors. The latter are designed to identify the following event topologies:

- Elastic scattering events: two collinear proton tracks, one on each side of the interaction point.
- Central diffractive events (Double Pomeron exchange): two non-collinear proton tracks, one on each side of the interaction point. The two proton can have different momenta.
- Single diffractive events: a proton track on one side only and tracks or energy depositions in the inner CMS or TOTEM detectors (T1 or T2) on the opposite side.

The estimated rates for these event classes at a luminosity of $10^{28} \text{ cm}^{-2} \text{ s}^{-1}$ are listed in Table 1. To tag any of them, the proton trigger on one side has to be combined with either a proton or an inelastic trigger on the other side. Since the TOTEM trigger and DAQ are synchronised with their CMS counterparts, the first-level trigger decision has to be taken within the CMS trigger latency of about $3 \mu\text{s}$ after the bunch crossing. Once proton travel and signal propagation times are taken into account only about 100 ns are left for the trigger decision.

The basic requirements for a highly efficient proton trigger providing an effective background rejection are the following:

- Selection of events with only one track per arm, this track being parallel to the outgoing beam within 0.1 mrad .
- A time resolution of about 5 ns to identify the bunch-crossing.
- A high efficiency up to the detector edge (within $20 \mu\text{m}$).

The last criterion plays an important role in the choice of a suitable detector technology. Different silicon detectors and scintillating fibers are under evaluation. Sufficient background rejection can be achieved with a trigger detector segmentation as wide as 1 mm .

The following backgrounds have to be considered:

- Beam halo: Due to the highly efficient LHC collimation system [5], needed for the protection of the superconducting magnets, the halo rate at 17σ away from the beam is expected not to exceed 3 kHz for the low luminosity runs. Hence, the fake coincidence rate between halo tracks on both sides of the IP will be about 20 Hz , still small compared to the allowed first-level trigger rate of 100 kHz .
- Beam-gas scattering: Based on expectations for the average residual gas density in the LHC beam pipe, the beam-gas interaction rate is about 100 Hz/m along the beam. Elastic beam-gas scattering is a part of the beam halo discussed above. Inelastic collisions produce many soft particles that will be swept away by the LHC magnets. Thus mainly particle showers produced in the ring section between the preceding quadrupole and the detector will contribute to the background. In the case of the Roman Pot station at 220 m the rate will be about 2 kHz . Most of these events will be eliminated at the first-level trigger with multiplicity and track angle cuts. The remaining background is small compared to the beam halo.
- Photons: The photon flux is much higher than the hadron flux and will amount to about 1 kHz/cm^2 . However, with a typical photon detection efficiency of 1% and a two-fold coincidence requirement within the same beam-pipe insertion, the rate is drastically reduced to about 0.03 Hz . Angular selections and a coin-

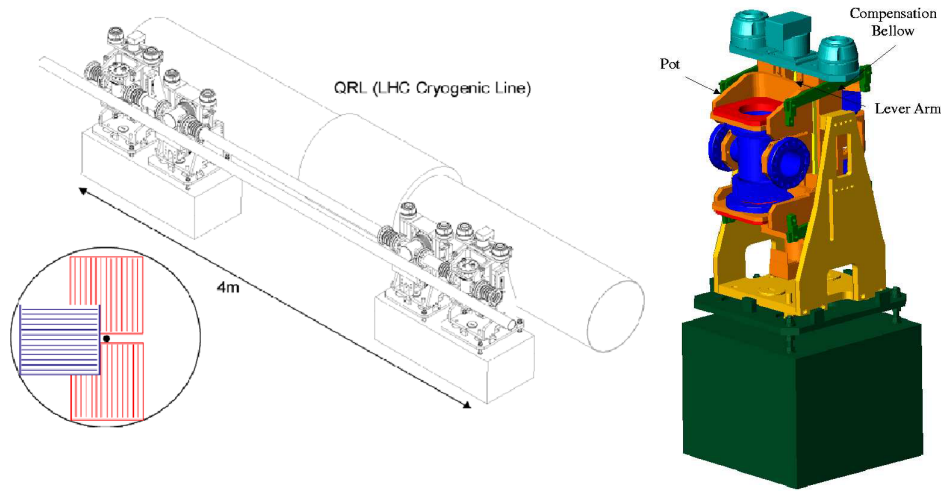


Fig. 8. (Left) A roman pot station in the tunnel of the LHC; the inset shows the overlap of the detectors in the vertical and horizontal pots. (Right) Details of a Roman Pot; the large mechanical structure is necessary to counterbalance the hydrostatic pressure on the movable section of the vacuum chamber

coincidence condition with the trigger detectors in a second beam-pipe insertion will further reduce the fake trigger rate.

In summary, the background is dominated by the beam halo (see Table 1). Its rate is small compared with the allowed first-level trigger rate.

A suitable trigger detector configuration consists of three planes per beam-pipe insertion. To avoid inefficiencies, only a two-out-of-three coincidence will be required. This concept also allows to monitor the efficiencies of the single detector planes.

2.2 Leading proton detection

The leading proton detectors are installed into special beam pipe insertions. The detector systems have to fulfill stringent requirements set by the LHC machine and the TOTEM experiment. A thin window separates the detector enclosure from the primary beam vacuum. The high intensity proton bunches pose a challenge concerning possible pick-up in the detectors close to the LHC beams. The detector systems have to be robust, aligned to within $20\mu\text{m}$ and their positions accurately maintained. Moreover, the detector systems have to withstand in the high-radiation environment of the LHC.

2.2.1 The Roman Pots

For optimal performance, the detectors should be active as close to their physical edge as possible. During operations they should be positioned at a distance of less than 1mm from the beam axis. First estimates indicate that a metallic shielding with thickness of about $200\mu\text{m}$ should be sufficient for both preventing RF pick-up problems and withstanding a possible pressure difference (caused by an accident) between the primary beam vacuum and the detector enclosure. A series of tests with full-scale prototype structures equipped with various thicknesses of an

INCONEL-718 shielding will be carried out at the end of 2003. Other walls of the Roman Pot, housing the proton detectors, are constructed of 3 mm thick stainless steel. The shielding foil is brazed to the steel frame and folded into its final shape. Tests of the brazing process are carried out together with an alternative method of electro erosion.

For LHC vacuum preservation, a NEG coating (non evaporable getter) is applied to the outer surfaces of the vacuum insertion. The pot should withstand the standard LHC bake-out temperature of 250°C . A thorough risk analysis of the proton detector enclosures and the moving mechanism will be carried out as requested by the LHC.

The Roman Pot, is designed to be as small as possible. Its attachment to the beam pipe insertion is accomplished by using a specially designed UHV flange (see Fig. 7). An optimal cooling system for the detectors is presently considered either using thin cooling pipe or cold fingers which bridges the heat load to a cold point outside the vacuum insertion. First estimates indicate that the added RF impedance due to the eight Roman Pots is negligible compared to the total LHC impedance budget ($250\text{m}\Omega$). The Roman Pot is designed to allow easy access to the detector system inside. A cantilever connects the moving mechanism of the insertion to the compensation bellows (Fig. 8).

The basic unit consists of two vertical Roman Pots (above and below the beam) movable in the vertical direction and a third one moving horizontally. By using the horizontal detector which overlaps with the vertical detectors when in measuring position, this arrangement allows to accurately measure the distance between the two vertical detectors on opposite sides of the beam (see Fig. 8). For efficient background rejection two units are installed within a distance of 4m (Fig. 8)

The radiation dose due to beam-beam interactions is calculated to be about 10^3Gy/year with a hadron fluence of approximately $10^9\text{cm}^{-2}\text{year}^{-1}$ [6]. All the detec-

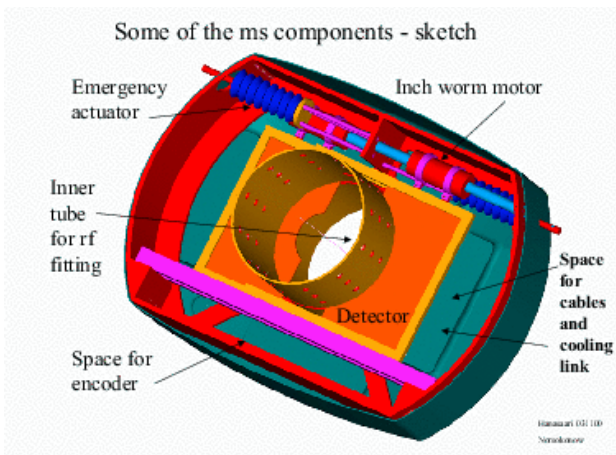


Fig. 9. A schematic drawing of the microstation including all the details except the thin window separating the secondary vacuum from the machine vacuum

tor components are foreseen to withstand the expected level of radiation at the luminosity of $10^{28} \text{ cm}^{-2} \text{ s}^{-1}$

2.2.2 The microstation

For location where the available space is too small to fit a traditional Roman Pot a Microstation (Ms) could be used instead.

By placing all the moving parts inside the vacuum, the force on them from the hydrostatic pressure is eliminated. This allows to build a system slightly larger than the detectors themselves.

The mechanical structure of a microstation is shown in Fig. 9, which illustrates the overall design with all the details. A microstation can be divided into four subsystems: the vacuum chamber, the support structure, the driving mechanism and the cooling system. An important feature of the design is to keep the stainless steel vacuum chamber independent of the precision mechanics and of the other components located inside. All the components are mounted on a support structure fixed only to the beam pipe inside the microstation such that any deformation of the vacuum chamber during the welding process or pump-down does not affect the rest of the system. The vacuum chamber can then be dimensioned to be as light as possible and the estimated total mass of the structure is less than 750 g.

2.3 Technologies for the leading proton detectors

The measurement of the elastic scattering to the smallest $|t|$ values also requires detectors efficient up to $20 \mu\text{m}$ to their physical edge.

In this section the technologies considered to build the edgeless elastic detectors are briefly described. The final choice on the technology will be made in 2004.

2.3.1 Cold Planar Silicon Detectors

Modern technologies for processing planar silicon detectors allow very fine segmentation. However, an insensitive border region extending several hundreds microns into the detector volume is needed for guard-rings which control the device's electric field and the surface leakage currents that may develop at the edge of the detector. In particular, if the detectors have to be exposed to high radiation doses, multi-guard-ring structures are required to allow a higher voltage operation to counterbalance radiation damage effects.

It was suggested that silicon planar detectors can be operated without guard rings if operated when cooled down to 130K [7]. Thus obtaining a drastic reduction of the inefficient material at the border of the detector. The successful measurement of the efficiency up to the edge of the silicon sensor has been performed with a microstrip detector cut through the sensitive area [8]. Scribing the backplane of a planar silicon detector with a laser beam and then bending it to crack produced a clean edge perpendicular to the strips. No further treatment was applied to the cut edge. The tracking efficiency near the cut edge was checked with a 120 GeV pion beam. For the measurement the detector under test was cooled to 110 K with a resulting leakage current of only 15 nA at full depletion voltage (45 V), then placed between two pairs of similar microstrip detectors mounted with their strips horizontal and vertical, V3 and H4 with V7 and H8 in Fig. 10.

The recorded hits on the reference planes and on the test detector allowed a fine study of the behaviour at the edge. The results (reproduced in Fig. 10(right)) show that the efficiency is uniform and reaches a maximum already at $25 \mu\text{m}$ from the physical edge. The data show that the position where the maximum is reached doesn't vary for different noise cuts. The uncertainty is dominated by the knowledge of the position of the detectors. It is worth noting that the beneficial effect of the low temperature operation also guarantees higher radiation hardness [9].

2.3.2 Cut planar silicon devices for operation at higher temperatures

In order to refine the construction process we are considering to implant on a $\text{p}^+ \text{-n-n}^+$ structure an n^+ ring that surrounds the sensitive area. For a fully depleted device with the n^+ ring set at the same potential as the back plane, the electric field is expected to reach the physical edge, if the carriers generation rate at the surface's edge is low. Nevertheless the leakage current due to thermal generation of carriers at the edge's surface can be controlled and kept low with a moderate decrease of the temperature. Detectors built according to this principle will be tested in a particle beam in a few months.

2.3.3 Edgeless 3D silicon detectors

"3D detectors" are silicon sensor built following a novel idea proposed by Sherwood Parker [10] of the University

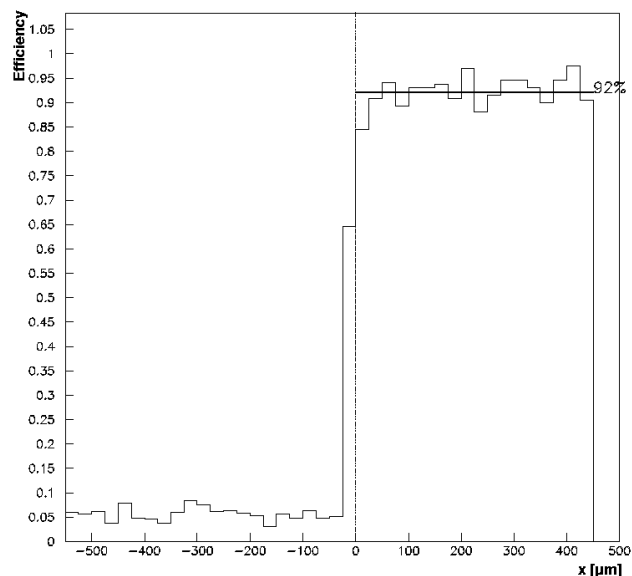
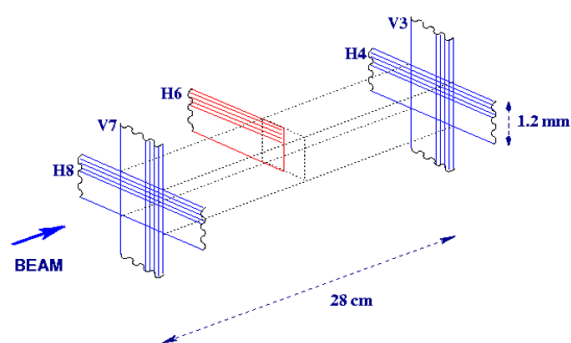


Fig. 10. The setup used for the beam test (*left*). Efficiency of the cut silicon detector: the efficiency rise coincides with the physical edge of the detector (*right*)

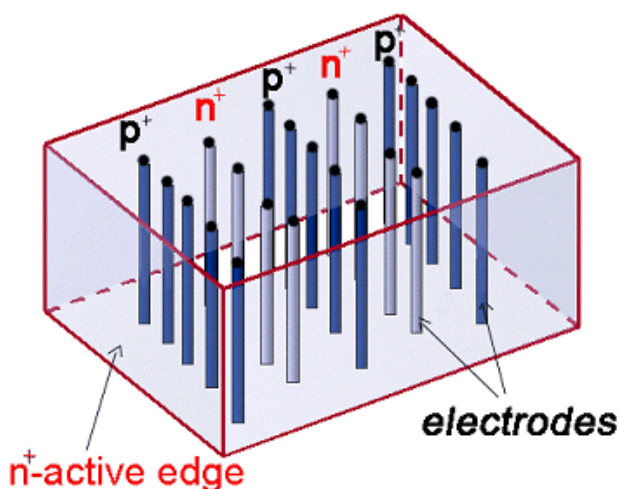


Fig. 11. In a 3D detector the electrodes and the active edges are fabricated inside the detector bulk using micromachining techniques

of Hawaii and colleagues in 1995 (see Fig. 11). These detectors have since been fabricated and fully characterised.

In this original configuration, the p^+ and n^+ electrodes are processed inside the bulk of the silicon wafer, rather than being implanted on its surface as in planar devices. The collaboration developing this new detector technology presently involve scientists from Brunel University in the UK, Hawaii and Stanford in the US.

The detector is built using deep reactive ion etching, developed for micro-electro-mechanical systems. By this technique micro-holes with a thickness-to-diameter ratio as large as 20:1 can be etched in silicon. In the 3D detectors presently processed holes are etched in wafers several

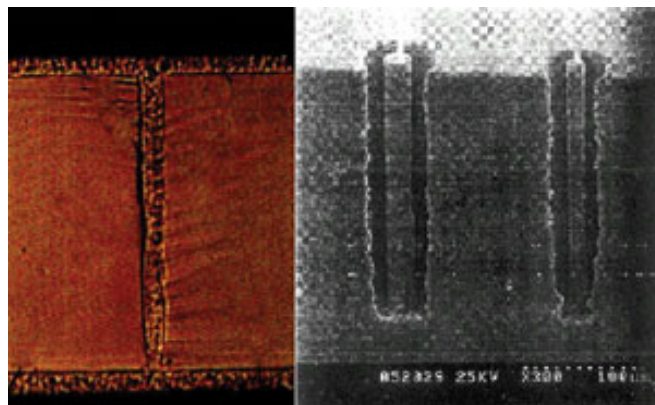


Fig. 12. *Right:* 290 μm deep C-shaped hole, filled with 2 μm polycrystalline silicon. The good quality of the etching and the uniformity of the deposition can be appreciated in the photo of a cut through the holes. *Left:* a cut wafer showing how the electrode looks after being filled with polysilicon

hundred microns thick, at distances as short as 50 μm from one another. During the fabrication the wafers are glued to a support substrate that will be removed at the end of the process.

The holes are then filled with polycrystalline silicon doped with either boron or phosphorus. Once the electrodes are filled, the polycrystalline silicon is removed from the surfaces, and the dopant is diffused into the surrounding single-crystal silicon to form the detector electrodes (Fig. 12). Aluminum is then deposited to provide contact with the electrodes in a pattern that will depend on how the individual electrodes are to be read out. Detectors fabricated with these dimensions can reach a spatial resolution of 10 – 15 μm .

The same micromachining technology can also be used to build detectors efficient up to the edge of the silicon.

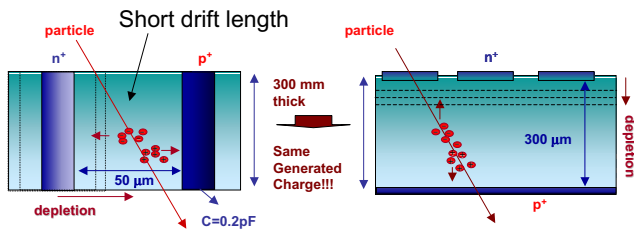


Fig. 13. A 3D detector design (*left*) compared to a standard planar detector (*right*)

Table 2. Comparison of parameters

Design Param.	3D	Planar
Depletion Voltage (V)	< 10	70
Collector length (μm)	~ 50	300
Charge collection time (ns)	1-2	10-20
Efficiency at ... μm from edge	< 10	~ 300

An *active-edge 3D sensor* was proposed in 1997 [12] and is also illustrated in Fig. 11. Prototypes have demonstrated efficient charge collection to within a few microns of their physical edges.

The schematic drawings in Fig. 13 compare the novel 3D design with the traditional planar one. Since the electric field is parallel (rather than orthogonal) to the detector surface, the charge¹ collection distance can be several times shorter, and the collection considerably faster. The voltage needed to extend the electric field throughout the volume between the electrodes (full depletion) can be an order of magnitude smaller (Table 2).

The signal generated by an ionizing particle traversing a 3D detector with all the electrodes connected together by an aluminum microstrip operated at 130 K shows a rise time of 1.5 ns with a pulse duration of 5 ns (Fig. 14 and [15]). A similarly fast response is observed at room temperature with 40 V bias voltage after the detector was exposed to a proton flux of 10^{15} cm^{-2} . The combination of short collection distance and high electric field increases the radiation tolerance of silicon detectors by possibly a factor of 10 if compared with planar devices. The improvement in radiation hardness is simply due to the geometrical dimensions of the collection area and might increase further by selecting properly the substrate materials.

The fast, radiation hard electronics used for this test was designed by the CERN microelectronics group [16]. The detectors will undergo more tests in a particle beam in the next months.

¹ For a $300 \mu\text{m}$ thick silicon wafer the charge generated by a traversing ionizing particle is approximately 24,000 electrons.

2.3.4 Active edges

Fig. 14 (right) shows a 3D detector made sensitive up to the physical edge. In 3D devices, the voltage at corresponding points on the top and bottom surfaces is equal, so there is no voltage drop across the edges. A thin *trench* is etched at the periphery of the 3D electrodes and then is filled like the other electrodes with suitably doped polycrystalline silicon to obtain the desired electric field distribution inside the active region of the detector. The resulting dead region at the edge is comparable in dimensions to the width of the trench and has been measured to be $\approx 5 \div 20 \mu\text{m}$.

2.3.5 Planar devices with active edges

The 3D technology allows to obtain very fast detectors, with very small pixels, with high intrinsic radiation hardness for room temperature operation and efficient very close to the physical edge. For applications like TOTEM where the very large pixel density is not necessary it is possible to simplify the construction process and obtain the required characteristics with a combination of planar and 3D technologies.

In the so called planar 3D devices the edge structure is replaced by an electrode that extends the n^+ back plane of the device to the front p^+ side. The active volume of the diode is, in this case, ‘enclosed’ in an equipotential electrode which controls the electric field lines and therefore the surface current.

This is obtained simply by etching a trench with a depth equal to the thickness of the device, polycrystalline silicon. Test detectors of this kind have been fabricated and preliminary, results show a dead area $< 20 \mu\text{m}$ from the physical edge.

These detectors are able to operate at room temperature thus eliminating the need for a delicate cooling system. These devices will also be tested soon in particles beam.

3 The inelastic scattering

The TOTEM experiment requires to measure simultaneously the elastic scattering and the total inelastic rate. Two main topologies of events can be identified among the inelastic processes: single diffractive (SD) and non-single-diffractive (NSD) events. Extrapolation from earlier data taken at lower energies and simulations with PYTHIA [19] (version 6.158) predict an inelastic cross-section $\sigma_{SD} \sim 14 \text{ mb}$ for the single diffractive and $\sigma_{NSD} \sim 65 \text{ mb}$ for non-single-diffractive processes which include *minimum bias* ($\sigma_{mb} \sim 55 \text{ mb}$) and double diffractive events ($\sigma_{DD} \sim 10 \text{ mb}$).

The TOTEM inelastic telescopes have been designed to detect the largest possible fraction of inelastic events and to provide a fully inclusive trigger. The telescopes will be installed symmetrically to the IP and have to be compatible with the CMS detector. Simulations show that in

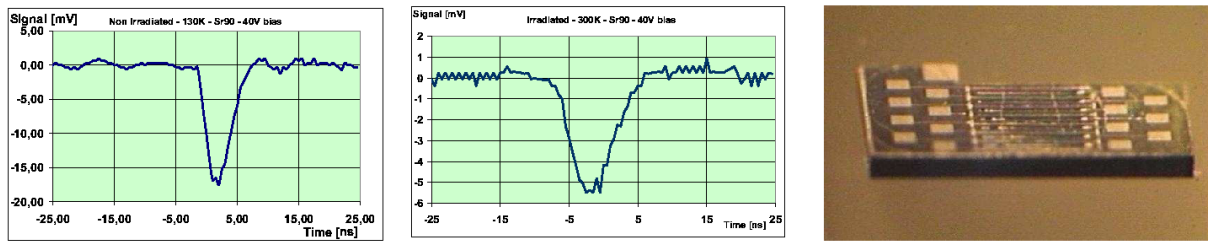


Fig. 14. *Left:* signals from ionizing particle traversing 3D detectors operated at 130 K show a rise times of 1.5 ns with a pulse duration of 5 ns. *Middle:* after heavy irradiation and at 300 K the rise time is 3.5 ns with a pulse duration of 10 ns. Bias voltage is 40 V in both cases. *Right:* complete 3D detector with aluminum microstrip pattern processed on one face; the active edge is clearly visible in front

the accessible pseudorapidity range $\sim 3.1 < \eta < \sim 6.8$ corrections and systematic errors can be controlled to obtain the needed precision. To cover the aforementioned rapidity range two detector telescopes are foreseen, T1 and T2. The T1 telescope will be placed in the CMS end-caps while T2 will be in the shielding behind the CMS Hadronic Forward (HF) calorimeter.

The telescopes for measuring inelastic events have a good trigger capability, provide tracking to identify beam-beam events and allow the measurement of the trigger efficiency. To discriminate beam-beam from beam-gas events the telescope will identify the primary interaction vertex with an accuracy at the level of a cm by reconstructing a few tracks from each side of the interaction point; the knowledge of the full event is not needed. NSD events are easily detected using a double-arm trigger which requires the coincidence of a left and right arm. The task becomes more challenging in the case of SD events. For these topologies tracks are in only one hemisphere and sometimes the multiplicity of the event is low. Moreover, a beam-gas event has a topology very similar to a SD event. The detection of a proton in the Roman Pots in the opposite arm makes SD trigger cleaner. It is expected that at least 95% of the inelastic events will be detected with very clean trigger conditions and the remaining fraction with a less clean trigger. The actual correction due to the losses will be evaluated by a Monte Carlo, properly tuned on the data themselves, keeping the final error below 1%.

3.1 The T1 telescope

3.1.1 Detector description

In order to reconstruct the event that has generated a trigger, 5 planes of Cathode Strip Chambers (CSC) [20] are installed in the End Cap of the CMS magnet. Each detector plane is composed of 6 trapezoidal detectors with sufficient overlap to obtain a uniform detection efficiency in ϕ . T1 will be built in two halves since installation in CMS will happen when the vacuum chamber is in place.

The proven detector technology allows to measure with one detector three independent coordinates for a track in one plane with sufficient precision even in the absence of a very accurate calibration.

The TOTEM CSC detector has one wire plane stretched between two facing and properly segmented cathode planes. To minimise the amount of material

traversed by the particles and yet maintain the necessary structural properties required, the cathode panels of TOTEM have a core of hexagonal Nomex honeycomb covered with very thin skins of 0.7 mm thickness (as compared to the 1.6 mm used for the CMS CSC). The electrodes on the cathode plane are etched on the thin copper layer by standard printed board technology. The strips are 4.0 mm wide and have 4.5 mm pitch, run parallel to one side of the detectors with an angle of 120° with respect to the anode wire direction. The two cathode planes are identical and are assembled in such a way that the cathode strips form an angle of 60° with respect to each other. The anode wire plane is supported by two properly shaped G-10 fiberglass bars of very precise thickness which are glued on one of the panels. The $30 \mu\text{m}$ diameter goldplated tungsten anode wires are soldered and then glued to this support with a pitch of 3 mm. The anode-cathode plane distance is (5.0 ± 0.1) mm.

3.1.2 Detector R/O

The T1 detectors have approximately 24k cathode strips and 12k anode wires in total.

The R/O electronic chain is based on the chips developed by the CMS Muon CSC group, however the R/O architecture has to be slightly different from the one in CMS. The CMS system is built to analyse, trigger and store the muon signals coming from 6 very close detectors whereas TOTEM needs to select and store the information of all the signals from 5 detectors planes installed over a distance of $2.8m$.

The signals from the anode wires, which are read individually, will provide a *Local Fast-OR* per detector to sample the cathode analogue information. All the anode-wire signals are brought together to determine a telescope trigger by coincidences between the planes, and to define – by using information from the different anode planes – the timing of the event. The identification of the bunch crossing of the event is not difficult for TOTEM since the bunch spacing of $2.5 \mu\text{s}$ in the high-beta optics will not cause any identification problems. However, in view of the use of the inelastic telescopes also during runs at higher luminosities (up to $10^{33} \text{ cm}^{-2}\text{s}^{-1}$), the system should identify the bunch crossing of a track segment. This configuration generates a data flow of a few Mbytes per second at a few hundred Hertz of trigger rate.

The radiation resistance of the electronics is one of the factors that will determine the maximum luminosity at which it will be possible to use the inelastic telescopes. Radiation levels are approximately two orders of magnitude higher in the T1 region than the levels at similar CMS muon End Cap detectors, given the larger η and the lack of shielding. However radiation is not a problem for the TOTEM specific runs which are at very low luminosity. The use of the T1 detector will be safe during the initial low-luminosity physics runs with normal optics foreseen for luminosity calibration. In case of long periods of high-luminosity runs, the telescope will be removed considering the relative ease with which T1 can be installed.

3.1.3 Installation in CMS

The T1 detector will be installed in a very delicate position inside the CMS detector, close to the vacuum chamber in both End Caps in front of the HF calorimeter. With its conic shape T1 fills the gap between the vacuum chamber and the iron of the End Cap, since it is the last device to be installed and consequently the first to be removed in case of access, the support structure had to be studied carefully: it has to allow installation in a very short time of less than 48 hours and comply with all the requirements set by the CMS Collaboration.

To minimize the clearance between the vacuum chamber and the detectors, the support of T1 must provide sufficient rigidity to hold the 2.8m long telescope with a weight of ≈ 150 kg (including cables, electronics and other services) with minimal deformations. Movements or deformation of the CMS End Caps due to the magnetic field operation or other causes are possible. To avoid them causing any unpredictable relative motion of T1 with respect to the vacuum chamber, the T1 support will be fixed only using the external disk of the CMS End Cap, i.e. the one by which the vacuum chamber is supported too. The support is a set of rails on a rigid frame fixed to the CMS End Cap. Detector half planes are in turn assembled on light frames that slide on the rails. Particular care was put into the study of the rail support frame, which has to fit inside the cone at $\eta = 3$, since its cross-section limits the space available to the T1 detectors.

The telescopes will be assembled on their installation platform which features a support frame with rails similar to the ones found in the CMS End Cap, and tested prior to their transport to the installation position where they will be aligned to the rails on the End Cap. The telescope will be transferred again on the transport platform for its removal. After the insertion of T1, the platform fixed on top of the CMS HF calorimeter will move up with the HF to its final position. The cable bundles from T1 are fed to the service racks on the platform through channels provided in the PE shielding plate which is present between the iron of the End Cap and the HF.

Detector half planes are held together by a *skeleton frame* of 3 mm thick aluminium sheets. Spacer plates keep the skeleton frames in their relative position, provide a minimum rigidity to the structure and support the elec-

tronics, the services and the cooling pipe to remove any extra heat from within the CMS volume.

3.1.4 CSC prototype tests in 2002

A prototype of the largest CSC with all the technical solutions foreseen for the construction of the final detectors has been built and tested.

Anodes were equipped with the CMS AD16 electronics while the cathodes were read out using the Gassiplex chip² digitised with a 12bit ADC. The detectors have operated in a very stable way and have shown a large HV plateau curve which is shown in Fig. 16 (left).

The residuals distribution for one cathode plane yields a spatial resolution $\sigma \approx 0.6$ mm which is sufficient for the reconstruction of the vertex of the inelastic event (see Fig. 16, right).

3.2 The T2 telescope

The T2 telescope complements the T1 telescope at larger η , an angular range dominated by the diffractive components of the inelastic interactions. With the present dimension of the vacuum pipe, the T2 telescope will cover with good efficiency the range $5.3 < \eta < 6.7$. This range is determined by the vacuum chamber and the edge of the HF calorimeter. Separating good beam-beam events from background becomes more difficult in this region because of the increased contribution of beam-gas scattering and the showering of particles and photons in the beam pipe as clearly indicated in the simulations (Fig. 19).

The telescope is installed about 13m from the IP inside the rotating shield of CMS with a maximum diameter of 50 cm (Fig. 17). The length and the spatial resolution of the detectors determine its vertex reconstruction capability. Considering that the dimensions of the detectors are not very large, the use of silicon detectors is conceivable. TOTEM may profit from the development and design work of the CMS and ATLAS trackers where large-area silicon detectors will be used.

A design is under study where silicon detectors identical to the ones in the forward disks of the CMS tracker are properly arranged to form a series of disks around the vacuum pipe. With the resolution provided by the detectors a good measurement of the vertex position at the IP can be obtained with a 50cm long telescope. In order to trigger the telescope at least two of the planes will be made with silicon pad detectors integrated with fast electronics. The chip under study provides a fast-or signal from 128 channels for fast trigger extraction and will have a multiplicity processor to reject special event topologies. The timing precision (~ 1 ns) is useful to identify the longitudinal position of the interaction point by the time of flight.

² developed for the ALICE Collaboration and slower than the final electronics foreseen for the read-out at LHC.

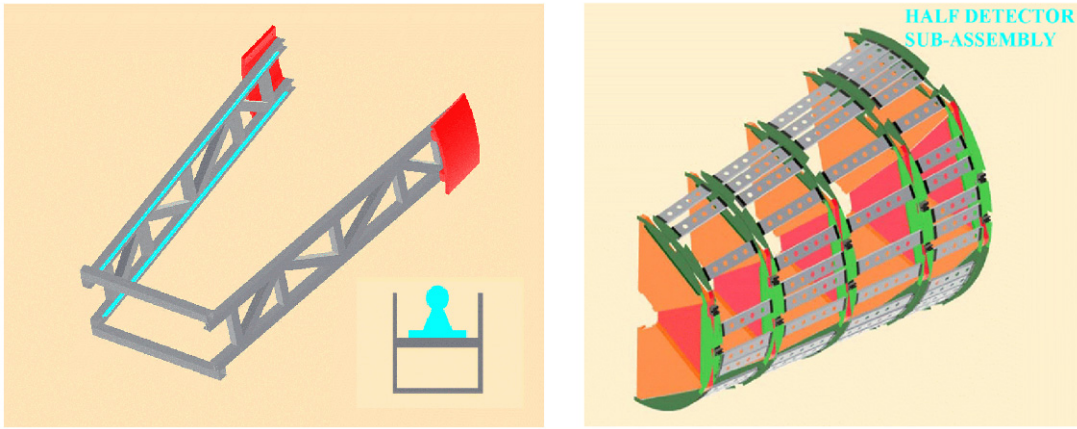


Fig. 15. *Left:* the support frame structure for the T1 telescope. *Right:* the half telescope

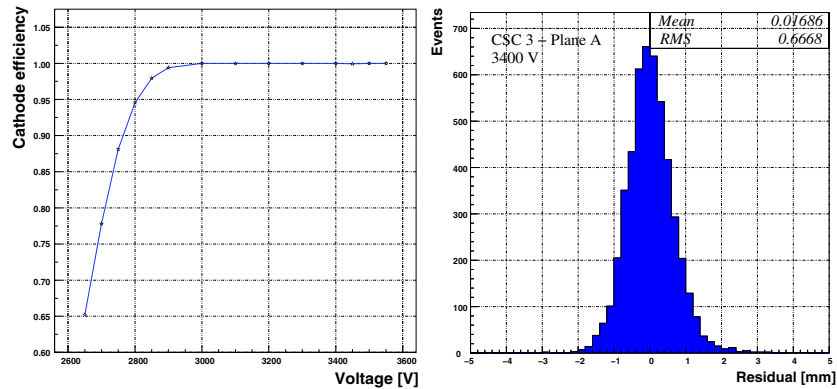


Fig. 16. Measurement of the efficiency of the TOTEM CSC detector as a function of the HV (*left*) and the spatial resolution (*right*)

3.3 The performance of the inelastic telescopes

The present design of the TOTEM inelastic telescopes T1 and T2 has been simulated by Geant4 [17] using OSCAR [18], the CMS framework for simulation. The beam-pipe description has been included in the simulation with its present shape, while the magnetic field was assumed to be turned off. A set of minimum bias events has been generated by Pythia 6.158 [19] and has been used as input for the simulation.

3.3.1 Geometrical acceptance and occupancy

The geometrical acceptance for the present design of T1 and T2 is shown in Fig. 18. The coverage of T1 in $|\eta|$ is from 3.1 to 4.6.

Simulated events allow to estimate the charged particle flux through T1 and T2 by counting the hits in each plane of the telescope (see Fig. 19). The upper line of the histogram represents the increase in the number of hits when the beam-pipe is included in the simulation. The charged particle multiplicity per event is shown in Fig. 20.

At a luminosity of $10^{28} \text{ cm}^{-2} \text{ s}^{-1}$ the flux through the first T1 plane is 1.5 Hz/cm^2 and decreases slightly to

0.6 Hz/cm^2 at the fifth whereas the flux through the first T2 plane is around 40 Hz/cm^2 .

For each CSC a mean strip/wire occupancy per event has been estimated. The strip occupancy it is around 6% for the long strips and it decreases below 1% for the shortest ones.

The wire occupancy depends only mildly on η and is about 4% for wires at high $|\eta|$ and about 2% for the others.

3.3.2 Pattern recognition

Pattern recognition plays an important role in the capability of the telescope to identify tracks and reconstruct the vertex of the interaction. Preliminary pattern recognition studies have focussed on finding track candidates and obtaining a fast evaluation of the *true* event multiplicity.

For pattern recognition the hits of the five detector planes are projected on an $\eta - \phi$ plane. This produces for each real track up to 15 uncorrelated coordinate points because of the stereo angle provided by the rotation of $\sim 3^\circ$ of each detector plane. Each plane measures the hit projections on three axes rotated by 120° with respect to each other. Measured points for tracks coming from

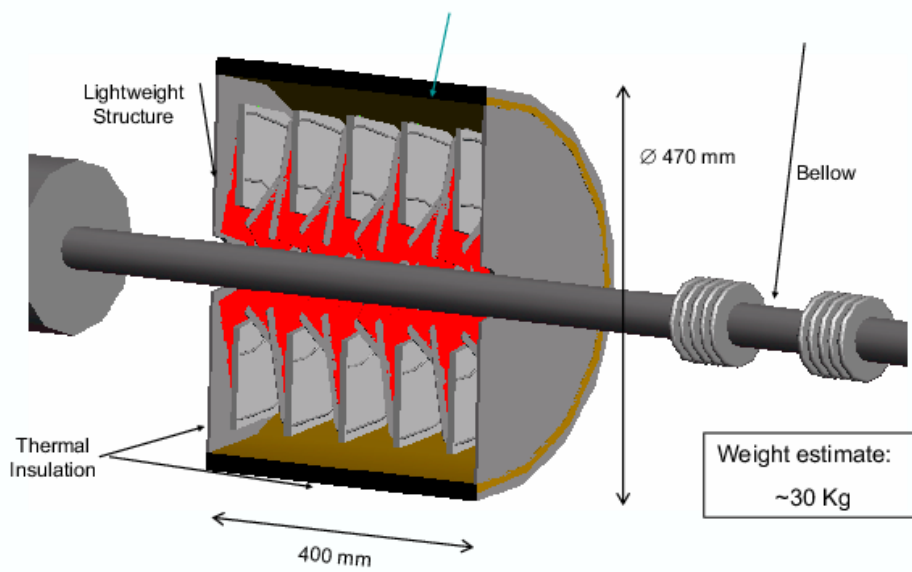


Fig. 17. The T2 telescope around the new CMS vacuum pipe

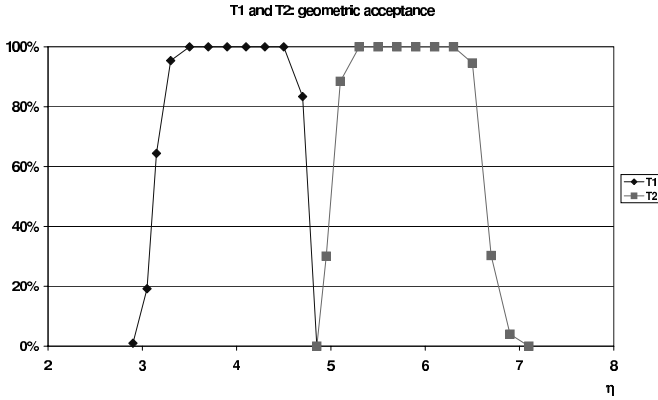


Fig. 18. Geometrical acceptance of T1 and T2

the interaction region should cluster in the same region. Points in the same region, or *road*, will be associated in the precise reconstruction of the tracks used to find the interaction vertex. A *road* in the $\eta - \phi$ plane has a size $0.6^\circ \times 1^\circ$. Each cell corresponds to a cone in the physical space with the vertex in the interaction point and with an opening $\Delta R = \sqrt{\Delta\eta^2 + \Delta\phi^2} = 1.17$.

Preliminary results indicate that by using the three measurements from the CSC (strips and wires) this method is very efficient in the identification of primary tracks with a very small probability of getting a fake track.

4 The luminosity measurement

The measurement of the total cross-section in the *high* β runs provides the absolute calibration of the machine luminosity, which can be expressed in terms of measurable

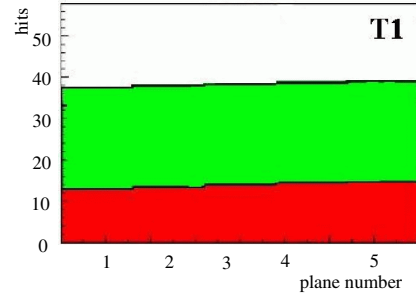


Fig. 19. Hits in the different detector planes of the TOTEM telescopes: the *top line* indicates the increase in the hit number due to the presence of the beam pipe

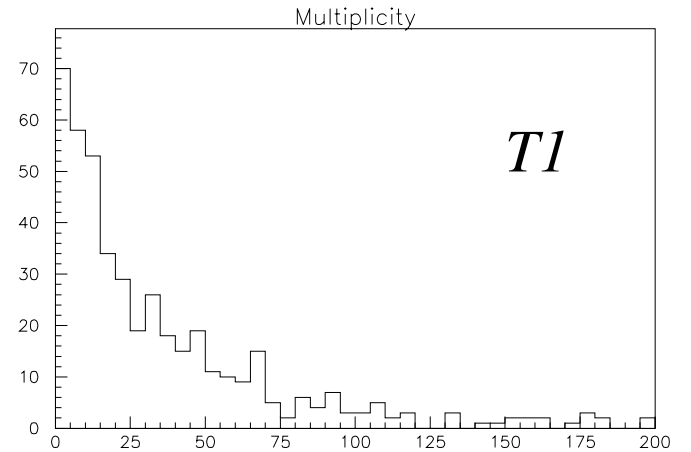


Fig. 20. Charged track multiplicity in telescope T1

quantities as:

$$\mathcal{L} = \frac{(1 + \varrho^2)}{16\pi} \frac{(N_{el} + N_{inel})^2}{(dN_{el}/dt)_{t=0}} \quad (5)$$

With the knowledge of the luminosity calibration any appropriate combination of TOTEM and CMS detectors can become a luminosity monitor, the only requirement being a negligible contamination from background events.

The absolute calibration of one monitor combination during the *high* β runs is made by measuring the total number N_{Mon} of monitor events to obtain the *effective* monitor cross-section as:

$$\sigma_{Mon} = \sigma_{tot} \left[\frac{N_{Mon}}{N_{el} + N_{inel}} \right] \quad (6)$$

The luminosity in normal LHC runs is given simply by:

$$\mathcal{L} = \frac{N_{Mon}}{\sigma_{Mon}} \quad (7)$$

Experience shows that a simple monitor is given by the coincidence of the two (left and right) T1 telescopes $T1_L \times T1_R$. The combination has high efficiency for NSD events and should not be strongly affected by background.

Various combinations of triggers will be monitored regularly and their relative stability will give an indication on the background conditions of each run.

4.1 CMS and extrapolation to higher luminosities

The calibration of specific Luminosity monitors from CMS is important in view of the measurement and monitoring of the luminosity for the high luminosity runs.

This was discussed in joint CMS/TOTEM meetings. In particular, two monitors have been explored in detail: the Tracker and the Hadronic Forward Calorimeter (HF).

For the tracker it is possible to reconstruct in an efficient and fast way the z-position of the interaction vertex using the 3 stereo layers of the barrel tracker. It has been shown [21] that the procedure will work properly, in the presence of pile-up, up to 5 events per bunch-crossing, i.e. a luminosity of $5 \times 10^{33} \text{ cm}^{-2}\text{s}^{-1}$. This fast reconstruction could be implemented also by hardware to provide an on-line luminosity measurement.

The second possibility is to count the number of HF sectors with some energy deposition. Different groupings (quadrants, sectors, single cells...) could be arranged for small to large luminosities. When the luminosity gets large it will be faster to count the number of sectors without hits (zero counting).

Other monitors based on specific physical processes will be cross-calibrated at intermediate luminosity to be-

come capable of luminosity monitoring when pile-up of events will pose a serious constraint on the measurement method.

References

1. The TOTEM collaboration, Letter of Intent, CERN/LHCC 97-49, LHCC/I 11 (1997).
2. The TOTEM collaboration, Technical Proposal, CERN/LHCC 99-7, LHCC/ P5 (1999).
3. C.Augier et al., Phys. Lett. B315 (1993) 503.
4. V.A. Khoze et al., Eur. Phys. J C18(2000)167.
5. R. Assmann et al.: Status of the LHC Collimation System, LEMIC talk, 8. April 2003, CERN.
6. N.V. Mokhov et al.: Accelerator Related Backgrounds in the LHC Forward Detectors, Fermilab-Conf-03/086, May 2003.
7. K.Borer et al., NIM A 440 (2000) 5; S.Grohman et al., IX Blois Work. on El. and Diff. Scatt., Pruhonice, Czech Republic, (2001), 363.
8. V. Avati et al., to be published, Proceedings of the 9th Pisa Meeting on Advanced Detectors - May 2003.
9. W.H. Bell et al., Proceedings 8th Pisa Meeting on Advanced Detectors - NIM A468 (2001).
10. S. I. Parker, C. J. Kenney and J. Segal, Nucl. Instr. Meth. A 395 328 (1997).
11. S. I. Parker and C. J. Kenney, IEEE Trans. on Nucl. Sci. 48 (5) 1629 (2001).
12. C. J. Kenney et al., IEEE Trans. on Nucl. Sci. 48 (2) 189 (2003).
13. C. J. Kenney, S. I. Parker and E. Walckiers, IEEE Trans. on Nucl. Sci. 48 (6) 2405 (2002).
14. C. J. Kenney et al, "First results of active-edge, planar, radiation sensors", Submitted to the IEEE, NSS, Portland, Oregon, October 2003.
15. C. Da Via, CERN Courier, Vol 43, Number 1, January 2003.
16. G. Anelli et al., "A high speed low noise transimpedance amplifier in a 0.25 μm CMOS technology", presented at ELMAU 2002, accepted for publication in Nucl. Instr. Meth. A.
17. <http://geant4.web.cern.ch/geant4/> .
18. <http://cmsdoc.cern.ch/oscar/> .
19. <http://www.thep.lu.se/~torbjorn/Pythia.html> .
20. CMS MUON Technical Design Report, CERN/LHCC 97-32, CMS TDR 3, 15 December 1997.
21. A. Starodumov, Talk at the "Joint CMS-TOTEM meeting on Luminosity measurement" 22/06/00, EDMS TOTEM-G-MIN-0001.